═══REVIEW COMMONS MANUSCRIPT═══

IMPORTANT:

- Manuscripts submitted to Review Commons are peer reviewed in a journal-agnostic way.
- Upon transfer of the peer reviewed preprint to a journal, the referee reports will be available in full to the handling editor.
- The identity of the referees will NOT be communicated to the authors unless the reviewers choose to sign their report.
- The identity of the referee will be confidentially disclosed to any affiliate journals to which the manuscript is transferred.

GUIDELINES:

- For reviewers: https://www.reviewcommons.org/reviewers
- For authors: https://www.reviewcommons.org/authors

CONTACT:

The Review Commons office can be contacted directly at: office@reviewcommons.org

Aromatase in adipose tissue exerts an osteoprotective function in male mice via phosphate regulation

Aoi Ikedo[1], Michiko Yamashita[2], Maiko Hoshino[3], Yosuke Okuno[4], Minori Uga[5], Kazuya Tanifuji[5], Hiroko Segawa[5], Seiji Fukumoto[6], Yuuki Imai[1, 7*]

[1]Division of Integrative Pathophysiology, Proteo-Science Center, Ehime University

[2]Department of Hepato-Biliary-Pancreatic Surgery and Breast Surgery, Ehime University Graduate School of Medicine

[3]Graduate School of Agriculture and Life Sciences, The University of Tokyo

[4]Department of Metabolic Medicine, Osaka University Graduate School of Medicine

[5]Department of Applied Nutrition, Tokushima University Graduate School of Biomedical Sciences

[6]Department of Molecular Endocrinology, Fujii Memorial Institute of Medical Sciences, Institute of Advanced Medical Sciences, Tokushima University

[7]Department of Pathophysiology, Ehime University Graduate School of Medicine.

*Yuuki Imai

Email: y-imai@m.ehime-u.ac.jp

Author Contributions: A.I., M.Y. and M.H. performed research, analyzed data, and wrote the paper. M.Y., M.H., Y.O., K.T., and M.U. performed research and analyzed data. H.S. designed research. S.F. designed research and wrote the paper. Y.I. conceived the study, designed research, and wrote the paper.

Competing Interest Statement: The authors declare no competing interest.

Keywords: Estrogen; aromatase; adipose tissue; osteoid; phosphate metabolism

Funding: This work was supported in part by Medical Research Grant, Takeda Science Foundation to A.I. and JSPS KAKENHI (JP23689066, JP15H04961, JP19H03786, JP22H03203, to Y.I.; JP19K18502, JP21K16688, to A.I.; JP22K09358 to Y.I., A.I.)

Abstract

Aromatase contributes to maintenance of bone mass because male patients with loss-of-function mutations of *CYP19A1* exhibit bone loss. Treatment with aromatase inhibitor also causes bone loss in men and post-menopausal women, suggesting that part of the anabolic effect of testosterone in men is dependent on estradiol (E2) biosynthesized by aromatase in non-gonadal tissues. It remains unclear how locally biosynthesized E2 contributes to maintenance of bone mass. We examined the function of aromatase in local tissues rather than gonads using cell-type specific aromatase knockout (KO) mice. Because osteoblast-specific aromatase KO mice exhibited no bone phenotype, we focused on adipose tissue, known as a reservoir of steroid hormones and analyzed the bone phenotypes of adipose tissue-specific aromatase KO mice ($Aro^{\Delta aP2}$). Sixteen-week-old male $Aro^{\Delta aP2}$ mice exhibited significantly lower bone mineral density in tibia and femur, especially in trabecular bone, than controls. Bone histomorphometry showed that $Aro^{\Delta aP2}$ mice exhibited an insufficient calcification bone phenotype with increased osteoid volume and width, and decreased osteoclast area and numbers. Moreover, serum phosphate, renal phosphate reabsorption and FGF23 were significantly lower in $Aro^{\Delta aP2}$, suggesting that the insufficient calcification phenotype in $Aro^{\Delta aP2}$ was not caused by excessive FGF23 activities. Finally, we analyzed NaPi2a and NaPi2c, phosphate transporters localized in the kidney, and found that protein levels in renal brush border membrane vesicles were lower in $Aro^{\Delta aP2}$. These results indicate that estrogens locally biosynthesized by aromatase in adipocytes can play a significant role in bone mass maintenance via regulation of phosphate reabsorption in the kidney by NaPi2.

59 **Impact Statement**

60 Male adipocyte-specific aromatase KO mice (*Aro*$^{\Delta aP2}$) exhibited bone loss and increased
61 osteoid due to decreased serum phosphate and urinary phosphate reabsorption as a
62 result of reduced NaPi2 proteins expression in the kidney.

63 **Introduction**

64 Postmenopausal osteoporosis is a major medical problem that reduces the quality of life
65 in elderly women (Rosen, 2005). Estrogen deficiencies can induce postmenopausal
66 osteoporosis due to the lack of various physiological functions of estrogen/estrogen
67 receptor signaling, such as maintenance of osteoclastic life span (Martin-Millan et al.,
68 2010; Nakamura et al., 2007), maintenance of osteoblast/osteocyte functions by Wnt
69 signaling (Almeida et al., 2013; Doolittle et al., 2022; Kondoh et al., 2014), inhibition of
70 inflammatory cytokine production (Pacifici, 2008), and negative feedback of FSH
71 secretion (Sun et al., 2006). Even in older men, low serum levels of estradiol (E2)
72 (Mellström et al., 2008) as well as testosterone (Shahinian, Kuo, Freeman, & Goodwin,
73 2005) can lead to significant risks of fractures. Estrogens are synthesized from
74 cholesterols by the activity of converting enzymes, including aromatase (*Cyp19a1*),
75 mainly in the gonads. The *Cyp19a1* gene is expressed in various tissues with
76 tissue-specific alternative splicing (Honda, Harada, & Takagi, 1994; Mahendroo,
77 Mendelson, & Simpson, 1993; Means, Kilgore, Mahendroo, Mendelson, & Simpson,
78 1991; Simpson et al., 1993). Patients harboring a loss-of-function mutation in the
79 *CYP19A1* gene show severe osteoporosis and greater stature due to delayed or
80 unsuccessful growth plate closure (Morishima, Grumbach, Simpson, Fisher, & Qin,
81 1995), both of which are sensitive to estrogen replacement therapy (Bilezikian,
82 Morishima, Bell, & Grumbach, 1998; Carani et al., 1997; Rochira & Carani, 2009).
83 Also, conventional aromatase knockout mice (ArKO) exhibited bone loss caused by
84 decreased bone formation (Oz et al., 2001) or increased bone resorption (Miyaura et al.,
85 2001). These reports indicate that the functions of aromatase are essential for the
86 preservation of bone health. However, it is still uncertain whether a deficiency of

87 aromatase alters bone metabolism directly or indirectly via systemic influences because
88 both patients and ArKO mice show systemic endocrine disturbances.
89 Aromatase inhibitors (AIs) are applied clinically to treat certain populations of breast
90 cancers in postmenopausal women (Goss et al., 2003). Although the serum levels of
91 estrogen should be remarkably decreased in postmenopausal women, AIs still have
92 adverse effects by increasing the risk of osteoporosis, called cancer treatment-induced
93 bone loss (Becker et al., 2012). Furthermore, Finkelstein et al. reported that the
94 administration of AIs to healthy men decreased bone mass in a serum testosterone
95 concentration-independent manner (Finkelstein et al., 2016). These results suggest that
96 part of the anabolic effect of testosterone (T) in men is dependent on E2 biosynthesis by
97 aromatase. This evidence may indicate that the activities of aromatase in peripheral
98 tissues and organs as well as the gonads are significant. Moreover, local synthesis of
99 estrogens by aromatase may exert a variety of biological functions. However, it remains
100 unclear how estrogens, which is biosynthesized locally by the action of aromatase in
101 non-gonadal tissues, contributes to the maintenance of bone mass.
102 In this study, we generated functional *Cyp19a1* floxed mice and osteoblast- or
103 adipocyte-specific aromatase KO mice. Male adipocyte-specific aromatase KO mice
104 ($Aro^{\Delta aP2}$) exhibited bone loss due to decreased serum phosphate and urinary phosphate
105 reabsorption as a result of reduced NaPi2 expression in kidney. These results indicate
106 that locally synthesized estrogens in adipocytes can play a significant role in bone mass
107 maintenance. It also suggests the possible existence of a new phosphate regulatory
108 mechanism through aromatase in adipose tissue.
109
110 **Results**

111 **Generation of *Cyp19a1* floxed mice.**

112 To assess the tissue-specific function of aromatase, which is coded by the *Cyp19a1* gene,
113 we generated *Cyp19a1* floxed mice. Figure S1 A shows the strategy used to generate the
114 mutant *Cyp19a1* allele. Two loxPs were designed to be inserted at sites flanking exon 8
115 and exon 9 of the *Cyp19a1* allele as those exons correspond to the catalytic domain of
116 aromatase (Ghosh, Griswold, Erman, & Pangborn, 2009). Successful insertion of NeoR
117 cassette and loxPs was confirmed by Southern blotting using two different probes
118 (Figure S1 B). Cre-mediated recombination excised exon 8, exon 9 and the NeoR gene
119 from the mutant allele, resulting in the null allele. As expected, the *Cyp19a1* transcript
120 was not detected in systemic *Cyp19a1* knockout ($Aro^{-/-}$) mice by either qualitative or
121 quantitative RT-PCR (Figure S1 C).

122

123 **Phenotypes of systemic and osteoblast-specific *Cyp19a1* knockout mice.**

124 To further confirm the abnormal phenotypes of the systemically expressed Cre-mediated
125 deletion in *Cyp19a1* floxed mice, we determined whether $Aro^{-/-}$ mice showed the same
126 phenotypic abnormalities reported in conventional *Cyp19a1* knockout mice (Fisher,
127 Graves, Parlow, & Simpson, 1998; Jones et al., 2000). As expected, female $Aro^{-/-}$ mice
128 exhibited smaller atrophic uteri and male $Aro^{-/-}$ mice showed significantly larger seminal
129 vesicles (Figure S1 D, E). Also, $Aro^{-/-}$ mice showed a significantly increased volume of
130 fat tissue, regardless of gender (Figure S1 E). These results suggested that aromatase
131 was functionally depleted in *Cyp19a1* floxed mice when excised by Cre-mediated
132 recombination of the *Cyp19a1* gene locus, as these phenotypes were similar to those in
133 previous reports.

134 Next, we tried to reveal the function of aromatase in osteoblast lineage cells, because

135 some previous studies reported that aromatase is expressed in osteoblasts (Sasano et al.,
136 1997; Shozu & Simpson, 1998; Yanase et al., 2003). We generated three lines of
137 osteoblast/osteocyte-specific *Cyp19a1* knockout mice by crossing *Cyp19a1* floxed
138 ($Aro^{flox/flox}$) mice with *2.3kb-Col1a1-Cre* ($Aro^{\Delta Col1a1}$), *OCN-Cre* ($Aro^{\Delta OCN}$), or *Dmp1-Cre*
139 ($Aro^{\Delta Dmp1}$) mice. Bone mineral density (BMD) in $Aro^{\Delta Col1a1}$ female mice and $Aro^{\Delta OCN}$
140 male mice was comparable with controls (Figure S2 A, B). In contrast, BMD of
141 $Aro^{\Delta Dmp1}$ mice was significantly greater in female but not male mice (Figure S2 C).
142 However, we did not analyze this phenotype in detail because our goal was to determine
143 why aromatase deficiency causes bone loss. Taken together, these results suggest that
144 local aromatase expression in osteoblast/osteocyte lineage cells either does not
145 contribute to bone mass maintenance or has a negative effect on bone mass.
146

147 **Deletion of *Cyp19a1* from adipose tissue resulted in decreased bone mass in male**
148 **mice.**

149 Adipose tissue is known as the major site of estrogen biosynthesis or restoration in
150 postmenopausal women and old men. Previous studies reported that aromatase
151 expression in adipose tissue was increased by age, obesity, and menopause (Agarwal,
152 Ashanullah, Simpson, & Bulun, 1997; Brown et al., 2017; Bulun & Simpson, 1994;
153 Mair, Gaw, & MacLean, 2020). To investigate the effects of expressed aromatase in
154 adipose tissue on bone, we generated adipocyte-specific *Cyp19a1* knockout mice
155 ($Aro^{\Delta aP2}$) by crossing $Aro^{flox/flox}$ mice with *aP2-Cre* mice. *Cyp19a1* expression levels in
156 epididymal white adipose tissue (eWAT) were significantly lower in $Aro^{\Delta aP2}$ compared
157 to controls (Figure 1 A). Although there were no differences in body weight (Figure 1
158 B), tibial and femoral BMD of $Aro^{\Delta aP2}$ male mice at the age of 16-20 weeks were

159 significantly lower compared to control but not female mice (Figure 1 C and Figure S2
160 D). Especially, proximal site BMD in the tibia was significantly less in $Aro^{\Delta aP2}$ mice
161 compared to controls. Also, $Aro^{\Delta aP2}$ mice had low gastrocnemius muscle weight, and
162 high eWAT weight compared to controls (Figure 1 D, E). These phenotypes of low bone
163 and high fat mass were also observed in $Aro^{\Delta aP2}$ mice at the age of 24 weeks (Figure S3
164 A-E). It has been reported that some Cre mouse lines develop skeletal dysplasia or
165 abnormal regeneration in tissues (Rodda & McMahon, 2006; Sakai et al., 2022).
166 Therefore, we tested whether these phenotypes of $Aro^{\Delta aP2}$ mice were due to the
167 influence of the Cre mouse line. The results showed that *aP2-Cre* mice were
168 comparable in tibial and femoral BMD, fat mass, and muscle mass to littermate WT
169 control mice (Figure S4 A-D). We measured adipocyte size in eWAT and performed
170 intraperitoneal glucose tolerance tests (IPGTT) because $Aro^{\Delta aP2}$ mice were obese.
171 Adipocyte size was no different between groups (Figure 1 F). Fasting blood glucose was
172 significantly higher overall in $Aro^{\Delta aP2}$ compared to controls, but there was no difference
173 at any specific time point between groups (Figure 1 G). Since $Aro^{\Delta aP2}$ mice have
174 suppressed E2 biosynthesis from T by aromatase in adipose tissue, serum T and E2
175 levels were measured by LC-MS/MS. There were no differences in serum E2 and T
176 levels between groups (Figure 1 H), suggesting that E2 biosynthesized by aromatase in
177 adipocytes works only locally, not systemically.
178 As E2 biosynthesis in adipocytes is reduced due to aromatase ablation in $Aro^{\Delta aP2}$, it is
179 presumed that E2/estrogen receptor (ER) signaling is also reduced. In fact, we examined
180 steroid hormone receptor expression in eWAT and found that *Esr1* expression was
181 significantly less in $Aro^{\Delta aP2}$ compared to control mice (Figure S5 A). Therefore, to
182 investigate whether the $Aro^{\Delta aP2}$ phenotype is due to local ERα action in adipocytes, we

183 generated adipose tissue-specific *Esr1* knockout mice (*ERα*$^{\Delta aP2}$) by crossing *ERα*$^{flox/flox}$
184 mice with *aP2-Cre* mice. *Esr1* expression levels in eWAT were significantly lower in
185 *ERα*$^{\Delta aP2}$ compared to control mice (Figure S5 B). The results showed no group
186 differences in body weight, bone or muscle mass (Figure S5 C, D, F). In contrast,
187 subcutaneous WAT (sWAT) and eWAT weight were significantly greater in *ERα*$^{\Delta aP2}$
188 compared to control mice (Figure S5 E). This phenotype was similar to that of *Aro*$^{\Delta aP2}$
189 mice. These results suggest that ERα in adipocytes is involved in lipid metabolism but
190 not bone metabolism. Therefore, the bone phenotype in *Aro*$^{\Delta aP2}$ was not an
191 ERα-mediated effect of adipocytes.
192
193 ***Aro*$^{\Delta aP2}$ mice had an abnormal phosphate metabolism.**
194 We analyzed bone structure and bone marrow fat volume of the proximal tibia of
195 *Aro*$^{\Delta aP2}$ and *Aro*$^{flox/flox}$ mice using μCT. Trabecular bone parameters such as trabecular
196 bone volume (BV/TV) and trabecular thickness (Tb.Th) were significantly lower in
197 *Aro*$^{\Delta aP2}$ compared to control mice (Figure 2 A). However, cortical bone parameters, and
198 regulated bone marrow tissue (rBMAT) volume were no different between groups
199 (Figure 2 B, C). Further, serum P1NP, a bone formation marker, and serum CTX, a bone
200 resorption marker, were no different between groups (Figure 2 D).
201 To investigate the dynamics of osteoclasts and osteoblasts, we performed bone
202 histomorphometry in the proximal tibia of *Aro*$^{\Delta aP2}$ and *Aro*$^{flox/flox}$ mice. Von Kossa
203 staining revealed significantly greater osteoid volume (OV/BV) and osteoid thickness
204 (O.Th) in *Aro*$^{\Delta aP2}$ compared to control mice (Figure 3 A, B). In addition, TRAP staining
205 revealed significantly lower osteoclast surface/bone surface (Oc.S/BS) and osteoclast
206 number/bone perimeter (N.Oc/B.Pm) in *Aro*$^{\Delta aP2}$ compared to control mice (Figure 3 G,

207 H). However, bone formation rate and osteoblast number were no different between
208 groups (Figure 3 C-F). These results suggest that $Aro^{\Delta aP2}$ mice exhibit an abnormal bone
209 calcification phenotype.
210 Dysregulated phosphate metabolism is an important cause for insufficient calcification.
211 To assess this, we analyzed serum and urine parameters related to phosphate
212 metabolism of $Aro^{\Delta aP2}$ and $Aro^{flox/flox}$ mice. Serum inorganic phosphate (IP) was
213 significantly lower in $Aro^{\Delta aP2}$ mice compared to control mice but not in urine (Figure 4
214 A, B). Other parameters in serum and urine such as calcium (Ca), alkaline phosphatase
215 (ALP), and creatinine (CRE) were no different between groups (Figure 4 A, B). Then
216 we calculated urinary phosphate reabsorption using serum and urine parameters.
217 Tmp/GFR, an indicator of phosphate reabsorption in the renal proximal tubules was
218 significantly lower in $Aro^{\Delta aP2}$ compared to control mice (Figure 4 C). In addition, serum
219 IP and OV/BV were significantly and negatively correlated (Figure 4 D). These results
220 suggest that $Aro^{\Delta aP2}$ mice have high osteoid volume and low bone mass due to
221 decreased serum IP caused by decreased urinary phosphate reabsorption.
222 To identify the responsible genes for the phenotypes due to lack of *Cyp19a1* in adipose
223 tissue that regulate phosphate metabolism, we performed RNA-seq analysis using total
224 RNA from eWAT in $Aro^{\Delta aP2}$ and $Aro^{flox/flox}$ mice. The PCA plot showed separation
225 between the $Aro^{\Delta aP2}$ and $Aro^{flox/flox}$ (Figure S6 A). The results yielded 125 genes with a
226 significant increase and 100 genes with a significant decrease (Figure S6 B). We
227 focused on the genes that showed significant changes and performed Gene Ontology
228 (GO) analysis. Genes involved in inflammatory responses were increased and genes
229 involved in nucleotide metabolic processes were decreased in $Aro^{\Delta aP2}$ compared to
230 controls (Figure S6 C, D), suggesting that the adipose tissue of $Aro^{\Delta aP2}$ mice was in an

231 inflammatory state and metabolically compromised. However, there were no genes
232 encoding proteins that act on other organs as a humoral factor among differentially
233 expressed genes.
234 Therefore, we decided to focus our analyses on existing and known factors that can
235 regulate phosphate metabolism. Phosphate reabsorption occurs in the proximal tubule
236 cells of the kidney, mainly via Na^+-Pi cotransporter 2a (NaPi2a) and Na^+-Pi
237 cotransporter 2c (NaPi2c). Phosphate homeostasis is under endocrine control that is
238 mediated by FGF23, PTH and 1,25-dihydroxyvitamin D (1α,25$(OH)_2D_3$) (Fukumoto &
239 Martin, 2009; Minisola et al., 2017). Of these, FGF23, PTH, and corticosterone
240 suppress NaPi2 expression or function in the renal tubule (Walton & Bijvoet, 1975). To
241 investigate why *Aro*$^{\Delta aP2}$ mice have low serum phosphate levels, we analyzed several
242 parameters that can be influenced by proximal tubular function and NaPi2 expression
243 levels in the kidney. Urine beta-2-microglobulin (B2M) and serum UA, indicators for
244 renal tubular damage, and Na, K, and CL, indicators for Fanconi syndrome, were no
245 different between groups (Figure 5 A-C). In addition, serum PTH, 1α,25$(OH)_2D_3$,
246 25$(OH)D_3$, and corticosterone were not different between groups (Figure 5 D, E, G). In
247 contrast, serum FGF23 levels were significantly lower in *Aro*$^{\Delta aP2}$ compared to control
248 mice (Figure 5 F). Initially we hypothesized that high FGF23, as seen in patients with
249 FGF23-related hypophosphatemic rickets/osteomalacia, was the cause of low phosphate
250 in *Aro*$^{\Delta aP2}$ mice. However, serum FGF23 probably decreased in response to lower serum
251 phosphate concentrations, suggesting that the insufficient calcification phenotype in
252 *Aro*$^{\Delta aP2}$ mice was not due to increased FGF23. Next, we analyzed NaPi2 expression in
253 the kidney. Transcript levels of *Npt2a* and *Npt2c* in the kidney were no different
254 between groups (Figure 5 H). As NaPi2 activity can be regulated by endocytosis and

255 membrane recycling of NaPi2 protein in addition to transcriptional and translational
256 regulations, protein levels of NaPi2a and NaPi2c in brush border membrane vesicles
257 (BBMVs) were confirmed by western blotting. Protein levels of NaPi2a and NaPi2c in
258 BBMVs were significantly decreased in $Aro^{\Delta aP2}$ compared to control mice (Figure 5 I).
259 In $Aro^{\Delta aP2}$ mice, phosphate-regulating hormones such as PTH, $1\alpha,25(OH)_2D_3$, and
260 corticosterone, previously reported to regulate NaPi2 in the kidney, were normal and
261 serum FGF23 was lower. Taken together, these results indicate that renal NaPi2 is
262 decreased in $Aro^{\Delta aP2}$ mice, independent of known NaPi2 regulation mechanisms.
263

264 **Discussion**

265 In this study, we investigated the osteoprotective function of aromatase in the
266 non-gonadal tissues, bone and adipose. Although three different types of
267 osteoblast/osteocyte-specific aromatase KO mice exhibited no low bone mass
268 phenotype, $Aro^{\Delta aP2}$ male mice but not female mice exhibited abnormal bone
269 calcification with low serum phosphate levels due to lower urinary phosphate
270 reabsorption caused by decreased NaPi2a and NaPi2c in the kidney (Figure 6).
271 Previous studies have demonstrated that obesity is associated with lower fracture risk.
272 In a reciprocal way, low body mass index (BMI) is associated with increased fracture
273 risk, mainly in the hip, but also in the spine, forearm and other sites, in post-menopausal
274 women (Mpalaris, Anagnostis, Goulis, & Iakovou, 2015). In addition, it has been
275 reported that increasing BMI was associated with a progressive increase in hip BMD
276 and structural measures in non-obese men, but no such improvements were seen in
277 obese men (BMI $\geq$ 30 kg/m^2) (Shen et al., 2015). These results suggest that moderate fat
278 mass is important to maintain bone mass and reduce fracture risk. These studies support

279 our data that E2 biosynthesized by aromatase in fat contributes to bone mass
280 maintenance. *Aro*$^{\Delta aP2}$ mice exhibited not only bone loss but also low muscle mass, high
281 fat mass, and high fasting blood glucose, partially similar to symptoms of late-onset
282 hypogonadism (LOH), an age-related androgen deficiency (Lunenfeld, Saad, & Hoesl,
283 2005). Furthermore, Finkelstein et al. examined changes in body composition
284 (Finkelstein et al., 2013) and bone mass (Finkelstein et al., 2016) in healthy men aged
285 20-50 years when the aromatization of T to E2 was inhibited using goserelin acetate
286 which suppresses endogenous gonadal steroid production, testosterone gel, and AIs such
287 as anastrozole. The results showed that inhibition of aromatization of T to E2 by
288 anastrozole increased the percentage of body fat (Finkelstein et al., 2013) and decreased
289 trabecular BMD as measured by quantitative computed tomography (Finkelstein et al.,
290 2016). These findings suggest that the effects of T are dependent on a predominantly
291 estrogenic effect for fat and bone in men. As the phenotype of *Aro*$^{\Delta aP2}$ mice was similar
292 to the results of these studies, estrogen, which is synthesized by aromatase in fat, could
293 play an important role in maintaining body composition as well as bone in men.
294 The present study suggested that *Aro*$^{\Delta aP2}$ mice have lower serum phosphate levels due to
295 lower urinary phosphate reabsorption caused by decreased NaPi2a and NaPi2c in the
296 kidney. Phosphate homeostasis is strictly regulated by hormones such as FGF23, PTH
297 and 1,25$(OH)_2D_3$. Among them, FGF23 was established as the principal hormone in
298 regulating blood phosphate level (Shimada et al., 2004). As a mechanism, FGF receptor
299 type 1 (FGFR1) works as a phosphate-sensing receptor, and its downstream intracellular
300 signaling pathway regulates the expression of *GALNT3*. And then, the post-translational
301 modifications of FGF23 protein via a gene product of *GALNT3* enhance FGF23
302 production. As results, FGF23 can reduce blood phosphate level by inhibiting both

303 proximal tubular phosphate reabsorption and intestinal phosphate absorption via
304 downregulating the activity of NaPi2a and NaPi2c in the kidney and blood
305 1α,25$(OH)_2D_3$ level (Takashi, 2024; Takashi et al., 2019; Takashi et al., 2021). However,
306 *Aro*$^{\Delta aP2}$ mice has normal phosphate-regulating hormones' level and low serum FGF23.
307 Therefore, the existence of novel control mechanisms other than those mentioned
308 factors above was suggested.
309 There are some limitations in this study. First, we tried to measure E2 level in fat tissue
310 by LC-MS/MS, but it could not be detected. Since ER signaling in eWAT was
311 significantly lower in *Aro*$^{\Delta aP2}$ compared to control mice, E2 was expected to be lower in
312 *Aro*$^{\Delta aP2}$. Second, we did not analyze patient data. There are no reports of low serum
313 phosphate levels in AI-treated patients or patients with loss-of-function mutations of the
314 *Cyp19a1* gene. However, as the phenotype in the present study was mild, it is expected
315 that the decrease in phosphate in patients might be a mild decrease within the reference
316 range. This requires further investigation. Third, we did not analyze *Aro*$^{\Delta aP2}$ female mice
317 in detail. It is hypothesized that the intact *Aro*$^{\Delta aP2}$ female mice had sufficient estrogen
318 production from the ovaries and thus had no phenotype (Figure S2 D). Therefore, it will
319 be necessary to analyze *Aro*$^{\Delta aP2}$ mice in which estrogen deficiency is induced by
320 ovariectomy or other means. Finally, in this study, we were unable to identify a novel
321 factor that regulates NaPi2 protein levels. All known predicted regulators were
322 examined, suggesting the existence of a novel phosphoregulatory mechanism that has
323 not been previously identified.
324 In conclusion, we have shown that E2 biosynthesis by aromatase in fat plays an
325 important role in the maintenance of bone mass in male via phosphate metabolism.
326

327 **Materials and Methods**

328 **Generation of *Cyp19a1* floxed mice by gene targeting.**

329 The PL451 vector, which contains a neo cassette flanked by two frt sites and one loxP
330 site, was obtained from NCI-Frederick. A cassette vector was generated by inserting the
331 second loxP site and the DT-A gene from the pMC1DTpA vector into PL451. Three
332 fragments containing the mouse *Cyp19a1* gene were amplified by PCR and inserted into
333 the cassette vector to form the final *Cyp19a1* knockout construct. The *Cyp19a1*
334 conditional knockout targeting vector was linearized by PmeI and was introduced into
335 M1 mouse embryonic cells (RIKEN) by electroporation and screened by genomic
336 Southern blotting. Probes for Southern blotting was amplified by PCR using the
337 following primers: Probe A, 5'-GGCCAGAGTCTGTCTGGAGT-3', and
338 5'-AAGCTCTGGCAGGTGTCAAT-3'; Probe B,
339 5'-ACCCAAAAGCCTCAACACAG-3', and 5'-GGCTTTCAGGACAAACCTTG-3'.
340 Chimeric mice were generated by aggregation of ES with eight cell embryos of BDF1
341 mice. Chimeric mice were crossed with wild-type C57BL/6J mice (CLEA Japan) and
342 the resulting pups with *Cyp19a1*$^{flox/+}$ were genotyped with the following primers:
343 5'-TAGGTGGCGAGAGAAAGGAA-3', and 5'-CCCCAGAGGCTTACACACAT-3'
344 (WT allele; 411 bps, floxed allele; 482 bps).

345

346 **Generation of systemic and osteoblast- or adipocyte- specific knockout mice.**

347 *Cyp19a1*$^{-/+}$ mice were generated by crossing *Cyp19a1*$^{flox/+}$ mice with *CMV-Cre* mice
348 (Dupé et al., 1997), which were kindly provided by Prof. Pierre Chambon. The null
349 allele was genotyped with the following primers: 5'-ATTCCCGCCGAATAATCTCT-3',
350 and 5'-ACCTTCCTTGACCAATGTCG-3' (Floxed [L2] allele; 6118 bps, KO [L-]

351 allele; 315 bps). *2.3kb-Col1a1-Cre* transgenic mice, which were kindly provided by Dr.
352 Gerard Karsenty (Dacquin, Starbuck, Schinke, & Karsenty, 2002), were crossed with
353 *Cyp19a1*$^{flox/flox}$ to generate *Aro*$^{\Delta Col1a1}$ mice. *Osteocalcin-Cre* mice (Zhang et al., 2002),
354 which were obtained from the Jackson Laboratory, were crossed with *Cyp19a1*$^{floxflox+}$ to
355 generate *Aro*$^{\Delta OCN}$ mice. *Dmp1-Cre* transgenic mice, kindly provided by Prof. Lynda
356 Bonewald (Lu et al., 2007), were crossed with *Cyp19a1*$^{floxflox+}$ to generate *Aro*$^{\Delta Dmp1}$ mice.
357 *aP2-Cre* mice (He et al., 2003), which were obtained from the Jackson Laboratory (JAX
358 stock #005069), were crossed with *Cyp19a1*$^{flox/flox}$ or *Esr1*$^{flox/flox}$ to generate *Aro*$^{\Delta aP2}$ or
359 *ERα*$^{\Delta aP2}$ mice. *Esr1*$^{flox/flox}$ mice were kindly provided by Prof. Chambon (Dupont et al.,
360 2000). Mice were housed in a specific pathogen-free facility under climate-controlled
361 conditions at room temperature (22 ± 2°C) with 25% humidity and a 12-hr light/dark
362 cycle. They were provided with ad libitum access to food and water. Animal
363 experiments were approved by the Animal Experiment Committee of Ehime University
364 (approval no. 37A1-1/16) and were performed in accordance with the Ehime University
365 Guidelines for Animal Experiments.
366

367 **RT-qPCR**

368 RNA was extracted from eWAT and kidney using a RNeasy Mini Kit (70146, QIAGEN)
369 with QIAzol Lysis Reagent (79306, QIAGEN) or ISOGEN (319-90211, NIPPON
370 GENE) and synthesized into cDNA using PrimeScript RT Master Mix (RR036, Takara
371 Bio Inc.). RT-qPCR was performed using cDNA to evaluate gene expression with
372 Thermal Cycler Dice (Takara Bio, Inc.) and SYBR Premix Ex Taq II (RR820S, Takara
373 Bio Inc.). *Rpl13a* or *Gapdh* was used as the housekeeping gene. Primers are shown in
374 Table S1.

375

376 **Radiological examination**

377 Samples were fixed in 4% paraformaldehyde phosphate buffer solution (PFA) overnight
378 at 4°C. The areal bone mineral density (aBMD) of the isolated tibiae and femora was
379 measured by Dual-energy X-ray absorptiometry (DXA) using a bone mineral analyzer
380 (DCS-600EX, ALOKA). Micro-computed tomography (μCT) scanning of the femora
381 was performed according to the manufacturer's instructions using a Scanco Medical
382 μCT35 System (SCANCO Medical) with an isotropic voxel size of 6 μm. We defined
383 the regions of interest (ROI) as 200 slices starting 1500 μm proximal to the proximal
384 growth plate in the tibia. These images were used for 3D reconstruction and analysis.
385 Structural parameters (3D) included cortical structure [bone area per total area (BA/TA),
386 BMD, and cortical thickness (Ct.Th)], and trabecular structure [bone volume per total
387 volume (BV/TV), trabecular number (Tb.N), trabecular thickness (Tb.Th), and BMD]
388 according to established guidelines (Bouxsein et al., 2010).

389

390 **Osmium staining**

391 Tibiae were harvested, fixed in 4% PFA overnight, and then immersed in 0.1 M EDTA
392 (pH 7.3) for 2 weeks for decalcification. The decalcified tibiae were immersed in a 1:1
393 mixture of 5% potassium dichromate and 2% osmium tetroxide (23310-10,
394 Polysciences, Inc., USA) for 48 h and stained. The stained tibiae were scanned using
395 μCT to evaluate marrow fat volume (Scheller et al., 2014).

396

397 **Histology and histomorphometry**

398 For bone histomorphometry, the mice were double labeled with subcutaneous injections

399 of 15 mg/kg of calcein (Sigma) at 4 and 2 days before sacrifice. Tibiae were removed
400 from each mouse and fixed with 4% PFA. After μCT analysis, tibiae were embedded
401 with Methylmethacrylate (MMA) after dehydration and the plastic sections were cut by
402 a standard microtome (LEICA) into 6 μm for Von Kossa, TRAP, and Toluidine blue
403 staining. The region of interest (ROI) was 750×1200 mm of secondary spongiosa in the
404 tibia. Each section was photographed using a cellSense Ver. 1.3 (OLYMPUS) and
405 analyzed using OsteoMeasure V3.3.0.1 (OsteoMetrics, Inc., GA, USA).
406

407 **Serum and urinary analysis**

408 Blood samples were collected from heart when mice were sacrificed. Blood samples
409 were centrifuged at 3,000 g at 4°C for 10 min, and separated serum samples were frozen
410 and stored at -80°C until analysis. Urine samples were collected for 24 hours on the day
411 before mice were sacrificed and stored at -80°C until analysis. Serum estradiol (E2),
412 testosterone (T), $1,25(OH)_2D_3$, and $25(OH)D_3$ were analyzed by LC-MS/MS. These
413 analyses were outsourced to ASKA Pharma Medical Co., Ltd. Serum P1NP
414 (MBS2702748, MyBioSource, Inc.), CTX (AC-06F1, Immunodiagnostic Systems),
415 PTH (60-2305, QuidelOrtho Corporation.), FGF23 (TCY4000 (11A735), KAINOS
416 Laboratories, Inc.), corticosterone (K014-H1/H5, Arbor Assays Inc.), and urine
417 beta-2-microglobulin (ab223590, abcam) were analyzed by ELISA respectively.
418 Analysis of serum IP, Ca, ALP, CRE, urine IP, Ca, and CRE were outsourced to Oriental
419 Yeast Co., ltd.
420

421 **Protein sample purification and immunoblotting**

422 BBMVs were prepared using the Ca^{2+} precipitation method. Cortical membrane and

423 whole homogenate were obtained from mouse kidneys and used for immunoblotting
424 analyses as described previously (Hanazaki et al., 2020; Ikuta et al., 2019; Ikuta et al.,
425 2018; Kaneko et al., 2018). Protein samples were heated at 95°C for 5 min in sample
426 buffer in the presence of 2-mercaptoethanol and subjected to sodium dodecyl
427 sulfate-polyacrylamide gel electrophoresis (SDS-PAGE). The separated proteins were
428 transferred by electrophoresis to Immobilon-P polyvinylidene difluoride membrane
429 (Millipore, Billerica, MA, USA) and treated with diluted antibodies. Signals were
430 detected using Immobilon Western (Millipore) (Hanazaki et al., 2020; Ikuta et al., 2019;
431 Ikuta et al., 2018; Kaneko et al., 2018). Rabbit anti-NaPi2a and NaPi2c polyclonal
432 antibodies were generated as described previously (Hanazaki et al., 2020; Segawa et al.,
433 2009; Segawa et al., 2005; Segawa et al., 2007). Mouse anti-actin monoclonal antibody
434 (MAB1501, Millipore, RRID: AB_2223041) was used as an internal control.
435 Horseradish peroxidase-conjugated anti-rabbit IgG was utilized as the secondary
436 antibody (115-035-003, Jackson ImmunoResearch Laboratories, Inc, West Grove, PA,
437 USA, RRID: AB_10015289). The diluted antibodies for immunoblotting were:
438 anti-NaPi2a (1:15,000), anti-NaPi2c (1:1500), and anti-actin (1:10,000).
439

440 **RNA-seq analysis**

441 Total RNA was extracted from eWAT using RNeasy Mini Kit (70146, QIAGEN) with
442 QIAzol Lysis Reagent (79306, QIAGEN). BRB-seq (Alpern et al., 2019) was performed
443 for preparing libraries with some following modifications. Oligo-dT based primer was
444 used for single-stranded synthesis and Second Strand Synthesis Module (NEB, #E6111)
445 was used for double-stranded cDNA synthesis. In-house MEDS-B Tn5 transposase
446 (Picelli et al., 2014; Sato et al., 2019) was used for tagmentation and amplified by 10

447 cycles of PCR using Phusion High-Fidelity DNA Polymerase (Thermo Scientific,
448 #M0530). 51bp of insert read (Read2) were obtained on Illumina NovaSeq6000.
449 Obtained FASTQ files were analyzed by RaNA-seq (Prieto & Barrios, 2020). Data were
450 registered in GEO with the accession number GSE263849. Gene Ontology Analysis
451 (GO) was conducted by DAVID (Huang da, Sherman, & Lempicki, 2009; Sherman et
452 al., 2022) for significantly ($p < 0.01$) changed genes.
453

454 **Statistical analysis**

455 The data are presented as means ± SD using unpaired t tests with Welch's correction.
456 The Brown-Forsythe and Welch ANOVA test was used for comparison among the four
457 groups, and Dunnett T3 was used for post-hoc analysis. Outliers were excluded by
458 Smirnov-Grubbs test. All statistical analyses were performed using Graph Pad Prism
459 Version 10.0.2 (GraphPad Software Inc., La Jolla, CA) and Microsoft Excel. P values
460 less than 0.05 were considered significant.
461

462 **Acknowledgments**

463 We are grateful to Dr. Erina Inoue for her technical support. We thank the staff of the
464 Division of Analytical Bio-Medicine and the Division of Laboratory Animal Research,
465 the Advanced Research Support Center (ADRES), the members of the Division of
466 Integrative Pathophysiology, Proteo-Science Center (PROS), and Ehime University for
467 their technical assistance and helpful support. We also thank the Medical Research
468 Center for High Depth Omics, Medical Institute of Bioregulation (MIB), Kyushu
469 University for the RNA-sequencing.
470

471 **Data Availability**

472 RNA-seq data have been deposited in the Gene Expression Omnibus as accession

473 number GSE263849.

References

Agarwal, V. R., Ashanullah, C. I., Simpson, E. R., & Bulun, S. E. (1997). Alternatively spliced transcripts of the aromatase cytochrome P450 (CYP19) gene in adipose tissue of women. *J Clin Endocrinol Metab, 82*(1), 70-74. doi:10.1210/jcem.82.1.3655

Almeida, M., Iyer, S., Martin-Millan, M., Bartell, S. M., Han, L., Ambrogini, E., . . . Manolagas, S. C. (2013). Estrogen receptor-α signaling in osteoblast progenitors stimulates cortical bone accrual. *J Clin Invest, 123*(1), 394-404. doi:10.1172/jci65910

Alpern, D., Gardeux, V., Russeil, J., Mangeat, B., Meireles-Filho, A. C. A., Breysse, R., . . . Deplancke, B. (2019). BRB-seq: ultra-affordable high-throughput transcriptomics enabled by bulk RNA barcoding and sequencing. *Genome Biol, 20*(1), 71. doi:10.1186/s13059-019-1671-x

Becker, T., Lipscombe, L., Narod, S., Simmons, C., Anderson, G. M., & Rochon, P. A. (2012). Systematic review of bone health in older women treated with aromatase inhibitors for early-stage breast cancer. *J Am Geriatr Soc, 60*(9), 1761-1767. doi:10.1111/j.1532-5415.2012.04107.x

Bilezikian, J. P., Morishima, A., Bell, J., & Grumbach, M. M. (1998). Increased bone mass as a result of estrogen therapy in a man with aromatase deficiency. *N Engl J Med, 339*(9), 599-603. doi:10.1056/nejm199808273390905

Bouxsein, M. L., Boyd, S. K., Christiansen, B. A., Guldberg, R. E., Jepsen, K. J., & Müller, R. (2010). Guidelines for assessment of bone microstructure in rodents using micro-computed tomography. *J Bone Miner Res, 25*(7), 1468-1486. doi:10.1002/jbmr.141

498 Brown, K. A., Iyengar, N. M., Zhou, X. K., Gucalp, A., Subbaramaiah, K., Wang, H., . . .
499 Dannenberg, A. J. (2017). Menopause Is a Determinant of Breast Aromatase
500 Expression and Its Associations With BMI, Inflammation, and Systemic Markers.
501 *J Clin Endocrinol Metab, 102*(5), 1692-1701. doi:10.1210/jc.2016-3606
502 Bulun, S. E., & Simpson, E. R. (1994). Competitive reverse transcription-polymerase
503 chain reaction analysis indicates that levels of aromatase cytochrome P450
504 transcripts in adipose tissue of buttocks, thighs, and abdomen of women increase
505 with advancing age. *J Clin Endocrinol Metab, 78*(2), 428-432.
506 doi:10.1210/jcem.78.2.8106632
507 Carani, C., Qin, K., Simoni, M., Faustini-Fustini, M., Serpente, S., Boyd, J., . . .
508 Simpson, E. R. (1997). Effect of testosterone and estradiol in a man with
509 aromatase deficiency. *N Engl J Med, 337*(2), 91-95.
510 doi:10.1056/nejm199707103370204
511 Dacquin, R., Starbuck, M., Schinke, T., & Karsenty, G. (2002). Mouse
512 alpha1(I)-collagen promoter is the best known promoter to drive efficient Cre
513 recombinase expression in osteoblast. *Dev Dyn, 224*(2), 245-251.
514 doi:10.1002/dvdy.10100
515 Doolittle, M. L., Saul, D., Kaur, J., Rowsey, J. L., Eckhardt, B., Vos, S., . . . Khosla, S.
516 (2022). Skeletal Effects of Inducible ERalpha Deletion in Osteocytes in Adult
517 Mice. *J Bone Miner Res, 37*(9), 1750-1760. doi:10.1002/jbmr.4644
518 Dupé, V., Davenne, M., Brocard, J., Dollé, P., Mark, M., Dierich, A., . . . Rijli, F. M.
519 (1997). In vivo functional analysis of the Hoxa-1 3' retinoic acid response
520 element (3'RARE). *Development, 124*(2), 399-410. doi:10.1242/dev.124.2.399
521 Dupont, S., Krust, A., Gansmuller, A., Dierich, A., Chambon, P., & Mark, M. (2000).

522 Effect of single and compound knockouts of estrogen receptors alpha (ERalpha)
523 and beta (ERbeta) on mouse reproductive phenotypes. *Development, 127*(19),
524 4277-4291.
525 Finkelstein, J. S., Lee, H., Burnett-Bowie, S. A., Pallais, J. C., Yu, E. W., Borges, L.
526 F., . . . Leder, B. Z. (2013). Gonadal steroids and body composition, strength,
527 and sexual function in men. *N Engl J Med, 369*(11), 1011-1022.
528 doi:10.1056/NEJMoa1206168
529 Finkelstein, J. S., Lee, H., Leder, B. Z., Burnett-Bowie, S. A., Goldstein, D. W., Hahn, C.
530 W., . . . Yu, E. W. (2016). Gonadal steroid-dependent effects on bone turnover
531 and bone mineral density in men. *J Clin Invest, 126*(3), 1114-1125.
532 doi:10.1172/JCI84137
533 Fisher, C. R., Graves, K. H., Parlow, A. F., & Simpson, E. R. (1998). Characterization of
534 mice deficient in aromatase (ArKO) because of targeted disruption of the cyp19
535 gene. *Proc Natl Acad Sci U S A, 95*(12), 6965-6970.
536 doi:10.1073/pnas.95.12.6965
537 Fukumoto, S., & Martin, T. J. (2009). Bone as an endocrine organ. *Trends Endocrinol*
538 *Metab, 20*(5), 230-236. doi:10.1016/j.tem.2009.02.001
539 Ghosh, D., Griswold, J., Erman, M., & Pangborn, W. (2009). Structural basis for
540 androgen specificity and oestrogen synthesis in human aromatase. *Nature,*
541 *457*(7226), 219-223. doi:10.1038/nature07614
542 Goss, P. E., Ingle, J. N., Martino, S., Robert, N. J., Muss, H. B., Piccart, M. J., . . . Pater,
543 J. L. (2003). A randomized trial of letrozole in postmenopausal women after five
544 years of tamoxifen therapy for early-stage breast cancer. *N Engl J Med, 349*(19),
545 1793-1802. doi:10.1056/NEJMoa032312

Hanazaki, A., Ikuta, K., Sasaki, S., Sasaki, S., Koike, M., Tanifuji, K., . . . Segawa, H. (2020). Role of sodium-dependent Pi transporter/Npt2c on Pi homeostasis in klotho knockout mice different properties between juvenile and adult stages. *Physiol Rep, 8*(3), e14324. doi:10.14814/phy2.14324

He, W., Barak, Y., Hevener, A., Olson, P., Liao, D., Le, J., . . . Evans, R. M. (2003). Adipose-specific peroxisome proliferator-activated receptor gamma knockout causes insulin resistance in fat and liver but not in muscle. *Proc Natl Acad Sci U S A, 100*(26), 15712-15717. doi:10.1073/pnas.2536828100

Honda, S., Harada, N., & Takagi, Y. (1994). Novel exon 1 of the aromatase gene specific for aromatase transcripts in human brain. *Biochem Biophys Res Commun, 198*(3), 1153-1160. doi:10.1006/bbrc.1994.1163

Huang da, W., Sherman, B. T., & Lempicki, R. A. (2009). Systematic and integrative analysis of large gene lists using DAVID bioinformatics resources. *Nat Protoc, 4*(1), 44-57. doi:10.1038/nprot.2008.211

Ikuta, K., Segawa, H., Hanazaki, A., Fujii, T., Kaneko, I., Shiozaki, Y., . . . Miyamoto, K. I. (2019). Systemic network for dietary inorganic phosphate adaptation among three organs. *Pflugers Arch, 471*(1), 123-136. doi:10.1007/s00424-018-2242-9

Ikuta, K., Segawa, H., Sasaki, S., Hanazaki, A., Fujii, T., Kushi, A., . . . Miyamoto, K. I. (2018). Effect of Npt2b deletion on intestinal and renal inorganic phosphate (Pi) handling. *Clin Exp Nephrol, 22*(3), 517-528. doi:10.1007/s10157-017-1497-3

Jones, M. E., Thorburn, A. W., Britt, K. L., Hewitt, K. N., Wreford, N. G., Proietto, J., . . . Simpson, E. R. (2000). Aromatase-deficient (ArKO) mice have a phenotype of increased adiposity. *Proc Natl Acad Sci U S A, 97*(23), 12735-12740. doi:10.1073/pnas.97.23.12735

570 Kaneko, I., Segawa, H., Ikuta, K., Hanazaki, A., Fujii, T., Tatsumi, S., . . . Miyamoto, K.
571 I. (2018). Eldecalcitol Causes FGF23 Resistance for Pi Reabsorption and
572 Improves Rachitic Bone Phenotypes in the Male Hyp Mouse. *Endocrinology,*
573 *159*(7), 2741-2758. doi:10.1210/en.2018-00109
574 Kondoh, S., Inoue, K., Igarashi, K., Sugizaki, H., Shirode-Fukuda, Y., Inoue, E., . . .
575 Imai, Y. (2014). Estrogen receptor α in osteocytes regulates trabecular bone
576 formation in female mice. *Bone, 60*, 68-77. doi:10.1016/j.bone.2013.12.005
577 Lu, Y., Xie, Y., Zhang, S., Dusevich, V., Bonewald, L. F., & Feng, J. Q. (2007).
578 DMP1-targeted Cre expression in odontoblasts and osteocytes. *J Dent Res, 86*(4),
579 320-325. doi:10.1177/154405910708600404
580 Lunenfeld, B., Saad, F., & Hoesl, C. E. (2005). ISA, ISSAM and EAU
581 recommendations for the investigation, treatment and monitoring of late-onset
582 hypogonadism in males: scientific background and rationale. *Aging Male, 8*(2),
583 59-74. doi:10.1080/13685530500163416
584 Mahendroo, M. S., Mendelson, C. R., & Simpson, E. R. (1993). Tissue-specific and
585 hormonally controlled alternative promoters regulate aromatase cytochrome
586 P450 gene expression in human adipose tissue. *J Biol Chem, 268*(26),
587 19463-19470.
588 Mair, K. M., Gaw, R., & MacLean, M. R. (2020). Obesity, estrogens and adipose tissue
589 dysfunction - implications for pulmonary arterial hypertension. *Pulm Circ, 10*(3),
590 2045894020952019. doi:10.1177/2045894020952023
591 Martin-Millan, M., Almeida, M., Ambrogini, E., Han, L., Zhao, H., Weinstein, R. S., . . .
592 Manolagas, S. C. (2010). The estrogen receptor-alpha in osteoclasts mediates the
593 protective effects of estrogens on cancellous but not cortical bone. *Mol*

Endocrinol, 24(2), 323-334. doi:10.1210/me.2009-0354

Means, G. D., Kilgore, M. W., Mahendroo, M. S., Mendelson, C. R., & Simpson, E. R. (1991). Tissue-specific promoters regulate aromatase cytochrome P450 gene expression in human ovary and fetal tissues. *Mol Endocrinol, 5*(12), 2005-2013. doi:10.1210/mend-5-12-2005

Mellström, D., Vandenput, L., Mallmin, H., Holmberg, A. H., Lorentzon, M., Odén, A., . . . Ohlsson, C. (2008). Older men with low serum estradiol and high serum SHBG have an increased risk of fractures. *J Bone Miner Res, 23*(10), 1552-1560. doi:10.1359/jbmr.080518

Minisola, S., Peacock, M., Fukumoto, S., Cipriani, C., Pepe, J., Tella, S. H., & Collins, M. T. (2017). Tumour-induced osteomalacia. *Nat Rev Dis Primers, 3*, 17044. doi:10.1038/nrdp.2017.44

Miyaura, C., Toda, K., Inada, M., Ohshiba, T., Matsumoto, C., Okada, T., . . . Ito, A. (2001). Sex- and age-related response to aromatase deficiency in bone. *Biochem Biophys Res Commun, 280*(4), 1062-1068. doi:10.1006/bbrc.2001.4246

Morishima, A., Grumbach, M. M., Simpson, E. R., Fisher, C., & Qin, K. (1995). Aromatase deficiency in male and female siblings caused by a novel mutation and the physiological role of estrogens. *J Clin Endocrinol Metab, 80*(12), 3689-3698. doi:10.1210/jcem.80.12.8530621

Mpalaris, V., Anagnostis, P., Goulis, D. G., & Iakovou, I. (2015). Complex association between body weight and fracture risk in postmenopausal women. *Obes Rev, 16*(3), 225-233. doi:10.1111/obr.12244

Nakamura, T., Imai, Y., Matsumoto, T., Sato, S., Takeuchi, K., Igarashi, K., . . . Kato, S. (2007). Estrogen prevents bone loss via estrogen receptor alpha and induction of

Fas ligand in osteoclasts. *Cell, 130*(5), 811-823. doi:10.1016/j.cell.2007.07.025

Oz, O. K., Hirasawa, G., Lawson, J., Nanu, L., Constantinescu, A., Antich, P. P., . . . Simpson, E. R. (2001). Bone phenotype of the aromatase deficient mouse. *J Steroid Biochem Mol Biol, 79*(1-5), 49-59. doi:10.1016/s0960-0760(01)00130-3

Pacifici, R. (2008). Estrogen deficiency, T cells and bone loss. *Cell Immunol, 252*(1-2), 68-80. doi:10.1016/j.cellimm.2007.06.008

Picelli, S., Björklund, A. K., Reinius, B., Sagasser, S., Winberg, G., & Sandberg, R. (2014). Tn5 transposase and tagmentation procedures for massively scaled sequencing projects. *Genome Res, 24*(12), 2033-2040. doi:10.1101/gr.177881.114

Prieto, C., & Barrios, D. (2020). RaNA-Seq: Interactive RNA-Seq analysis from FASTQ files to functional analysis. *Bioinformatics, 36*(6), 1955-1956. doi:10.1093/bioinformatics/btz854

Rochira, V., & Carani, C. (2009). Aromatase deficiency in men: a clinical perspective. *Nat Rev Endocrinol, 5*(10), 559-568. doi:10.1038/nrendo.2009.176

Rodda, S. J., & McMahon, A. P. (2006). Distinct roles for Hedgehog and canonical Wnt signaling in specification, differentiation and maintenance of osteoblast progenitors. *Development, 133*(16), 3231-3244. doi:10.1242/dev.02480

Rosen, C. J. (2005). Clinical practice. Postmenopausal osteoporosis. *N Engl J Med, 353*(6), 595-603. doi:10.1056/NEJMcp043801

Sakai, H., Sawada, Y., Tokunaga, N., Tanaka, K., Nakagawa, S., Sakakibara, I., . . . Imai, Y. (2022). Uhrf1 governs the proliferation and differentiation of muscle satellite cells. *iScience, 25*(3), 103928. doi:10.1016/j.isci.2022.103928

Sasano, H., Uzuki, M., Sawai, T., Nagura, H., Matsunaga, G., Kashimoto, O., & Harada,

642 N. (1997). Aromatase in human bone tissue. *J Bone Miner Res, 12*(9),
643 1416-1423. doi:10.1359/jbmr.1997.12.9.1416
644 Sato, S., Arimura, Y., Kujirai, T., Harada, A., Maehara, K., Nogami, J., . . . Kurumizaka,
645 H. (2019). Biochemical analysis of nucleosome targeting by Tn5 transposase.
646 *Open Biol, 9*(8), 190116. doi:10.1098/rsob.190116
647 Scheller, E. L., Troiano, N., Vanhoutan, J. N., Bouxsein, M. A., Fretz, J. A., Xi, Y., . . .
648 Horowitz, M. C. (2014). Use of osmium tetroxide staining with
649 microcomputerized tomography to visualize and quantify bone marrow adipose
650 tissue in vivo. *Methods Enzymol, 537*, 123-139.
651 doi:10.1016/B978-0-12-411619-1.00007-0
652 Segawa, H., Onitsuka, A., Furutani, J., Kaneko, I., Aranami, F., Matsumoto, N., . . .
653 Miyamoto, K. (2009). Npt2a and Npt2c in mice play distinct and synergistic
654 roles in inorganic phosphate metabolism and skeletal development. *Am J Physiol*
655 *Renal Physiol, 297*(3), F671-678. doi:10.1152/ajprenal.00156.2009
656 Segawa, H., Yamanaka, S., Ito, M., Kuwahata, M., Shono, M., Yamamoto, T., &
657 Miyamoto, K. (2005). Internalization of renal type IIc Na-Pi cotransporter in
658 response to a high-phosphate diet. *Am J Physiol Renal Physiol, 288*(3),
659 F587-596. doi:10.1152/ajprenal.00097.2004
660 Segawa, H., Yamanaka, S., Onitsuka, A., Tomoe, Y., Kuwahata, M., Ito, M., . . .
661 Miyamoto, K. (2007). Parathyroid hormone-dependent endocytosis of renal type
662 IIc Na-Pi cotransporter. *Am J Physiol Renal Physiol, 292*(1), F395-403.
663 doi:10.1152/ajprenal.00100.2006
664 Shahinian, V. B., Kuo, Y. F., Freeman, J. L., & Goodwin, J. S. (2005). Risk of fracture
665 after androgen deprivation for prostate cancer. *N Engl J Med, 352*(2), 154-164.

666 doi:10.1056/NEJMoa041943
667 Shen, J., Nielson, C. M., Marshall, L. M., Lee, D. C., Keaveny, T. M., & Orwoll, E. S.
668 (2015). The Association Between BMI and QCT-Derived Proximal Hip
669 Structure and Strength in Older Men: A Cross-Sectional Study. *J Bone Miner*
670 *Res, 30*(7), 1301-1308. doi:10.1002/jbmr.2450
671 Sherman, B. T., Hao, M., Qiu, J., Jiao, X., Baseler, M. W., Lane, H. C., . . . Chang, W.
672 (2022). DAVID: a web server for functional enrichment analysis and functional
673 annotation of gene lists (2021 update). *Nucleic Acids Res, 50*(W1), W216-w221.
674 doi:10.1093/nar/gkac194
675 Shimada, T., Hasegawa, H., Yamazaki, Y., Muto, T., Hino, R., Takeuchi, Y., . . .
676 Yamashita, T. (2004). FGF-23 is a potent regulator of vitamin D metabolism and
677 phosphate homeostasis. *J Bone Miner Res, 19*(3), 429-435.
678 doi:10.1359/jbmr.0301264
679 Shozu, M., & Simpson, E. R. (1998). Aromatase expression of human osteoblast-like
680 cells. *Mol Cell Endocrinol, 139*(1-2), 117-129.
681 doi:10.1016/s0303-7207(98)00069-0
682 Simpson, E. R., Mahendroo, M. S., Means, G. D., Kilgore, M. W., Corbin, C. J., &
683 Mendelson, C. R. (1993). Tissue-specific promoters regulate aromatase
684 cytochrome P450 expression. *J Steroid Biochem Mol Biol, 44*(4-6), 321-330.
685 doi:10.1016/0960-0760(93)90235-o
686 Sun, L., Peng, Y., Sharrow, A. C., Iqbal, J., Zhang, Z., Papachristou, D. J., . . . Zaidi, M.
687 (2006). FSH directly regulates bone mass. *Cell, 125*(2), 247-260.
688 doi:10.1016/j.cell.2006.01.051
689 Takashi, Y. (2024). Phosphate-sensing mechanisms and functions of phosphate as a first

690 messenger. *Endocr J*. doi:10.1507/endocrj.EJ24-0082

691 Takashi, Y., Kosako, H., Sawatsubashi, S., Kinoshita, Y., Ito, N., Tsoumpra, M. K., . . .
692 Fukumoto, S. (2019). Activation of unliganded FGF receptor by extracellular
693 phosphate potentiates proteolytic protection of FGF23 by its O-glycosylation.
694 *Proc Natl Acad Sci U S A, 116*(23), 11418-11427. doi:10.1073/pnas.1815166116

695 Takashi, Y., Sawatsubashi, S., Endo, I., Ohnishi, Y., Abe, M., Matsuhisa, M., . . .
696 Fukumoto, S. (2021). Skeletal FGFR1 signaling is necessary for regulation of
697 serum phosphate level by FGF23 and normal life span. *Biochem Biophys Rep,*
698 *27*, 101107. doi:10.1016/j.bbrep.2021.101107

699 Walton, R. J., & Bijvoet, O. L. (1975). Nomogram for derivation of renal threshold
700 phosphate concentration. *Lancet, 2*(7929), 309-310.
701 doi:10.1016/s0140-6736(75)92736-1

702 Yanase, T., Suzuki, S., Goto, K., Nomura, M., Okabe, T., Takayanagi, R., & Nawata, H.
703 (2003). Aromatase in bone: roles of Vitamin D3 and androgens. *The Journal of*
704 *Steroid Biochemistry and Molecular Biology, 86*(3-5), 393-397.
705 doi:10.1016/s0960-0760(03)00349-2

706 Zhang, M., Xuan, S., Bouxsein, M. L., von Stechow, D., Akeno, N., Faugere, M. C., . . .
707 Clemens, T. L. (2002). Osteoblast-specific knockout of the insulin-like growth
708 factor (IGF) receptor gene reveals an essential role of IGF signaling in bone
709 matrix mineralization. *J Biol Chem, 277*(46), 44005-44012.
710 doi:10.1074/jbc.M208265200

711

712 **Figures**

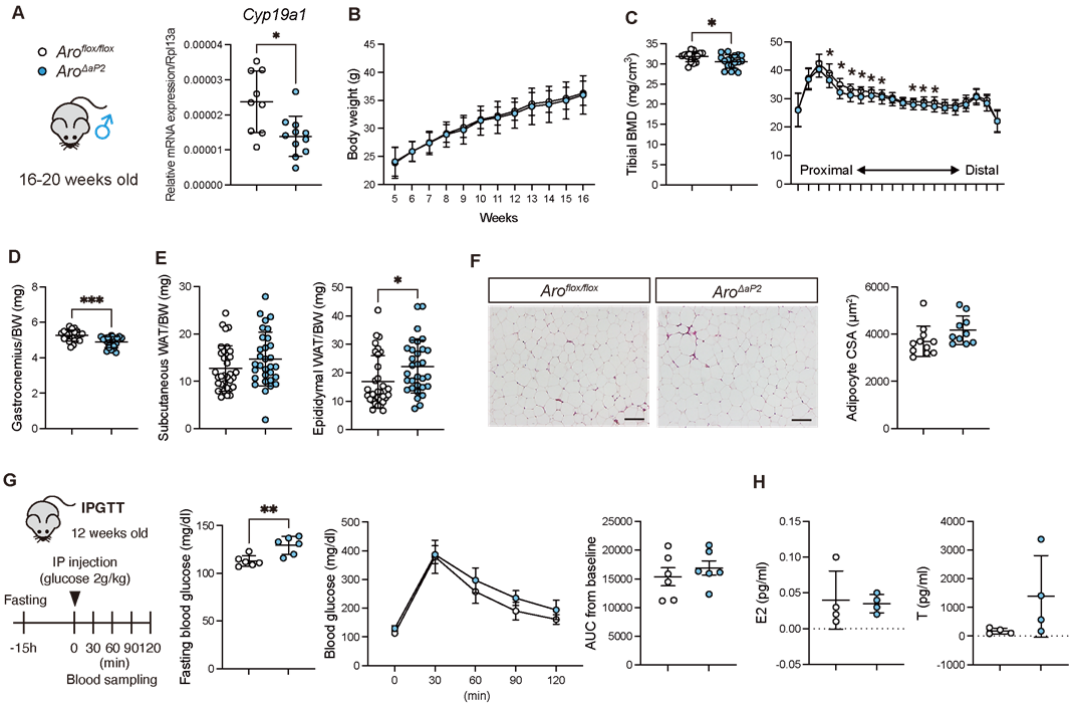

713

714 **Figure 1.** Male *Aro*$^{\Delta aP2}$ mice exhibited low bone mass, low muscle mass, high fat mass,
715 and high fasting blood glucose. (A) *Cyp19a1* gene expression in eWAT. (B) Body
716 weight. (C) Total tibial BMD (left) and BMD at each site when the bone is divided into
717 20 sections (right). (D) Gastrocnemius muscle weight per body weight. (E)
718 Subcutaneous and epidydimal white adipose tissue weight per body weight. (F)
719 Representative image and quantitative data of adipocyte cross sectional area (CSA) in
720 eWAT. Scale bar indicates 100 μm. (G) Intraperitoneal glucose tolerance test (IPGTT)
721 of 12 weeks old *Aro*$^{\Delta aP2}$ and *Aro*$^{flox/flox}$ mice. (H) Serum estradiol (E2) and testosterone
722 (T) by LC-MS/MS. Data are presented as means ± SD. *, $p < 0.05$; **, $p < 0.01$; ***, p
723 < 0.001

724

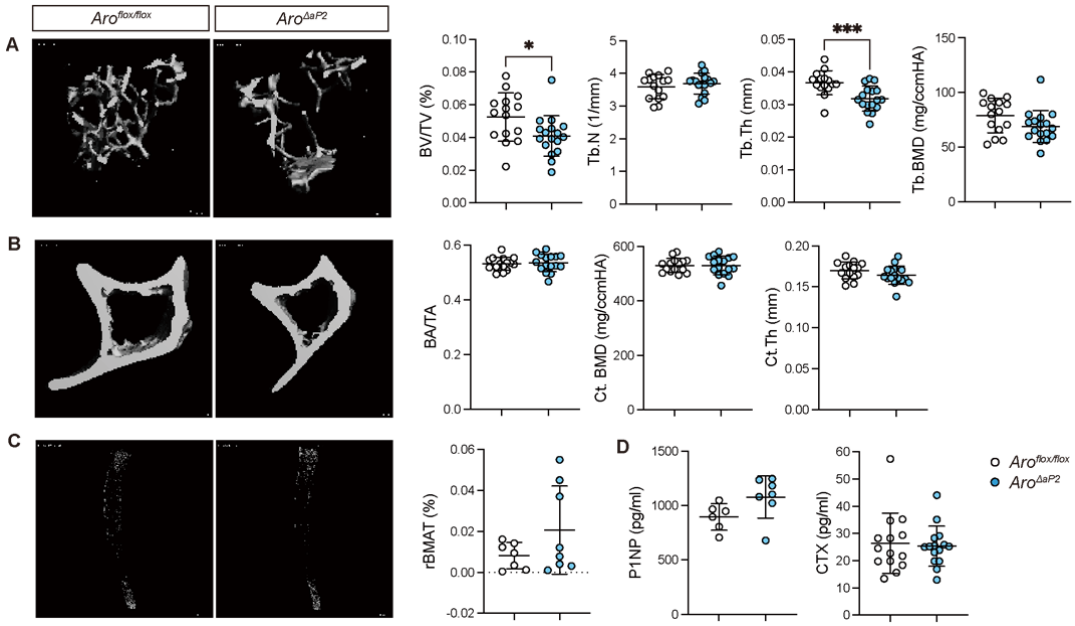

725

726 **Figure 2.** *Aro*$^{\Delta aP2}$ mice exhibited low trabecular bone volume at the proximal tibia.
727 Representative image and quantitative data of (A) bone volume per tissue volume
728 (BV/TV), trabecular number (Tb.N), trabecular thickness (Tb.Th), and trabecular bone
729 mineral density (Tb.BMD) as trabecular bone parameters, (B) bone area per tissue area
730 (BA/TA), cortical bone mineral density (Ct.BMD), and cortical thickness (Ct.Th) as
731 cortical bone parameters, and (C) regulated bone marrow tissue (rBMAT) volume at the
732 proximal tibia. (D) Serum P1NP and CTX concentration. Data are presented as means ±
733 SD. *, $p < 0.05$; ***, $p < 0.001$

734

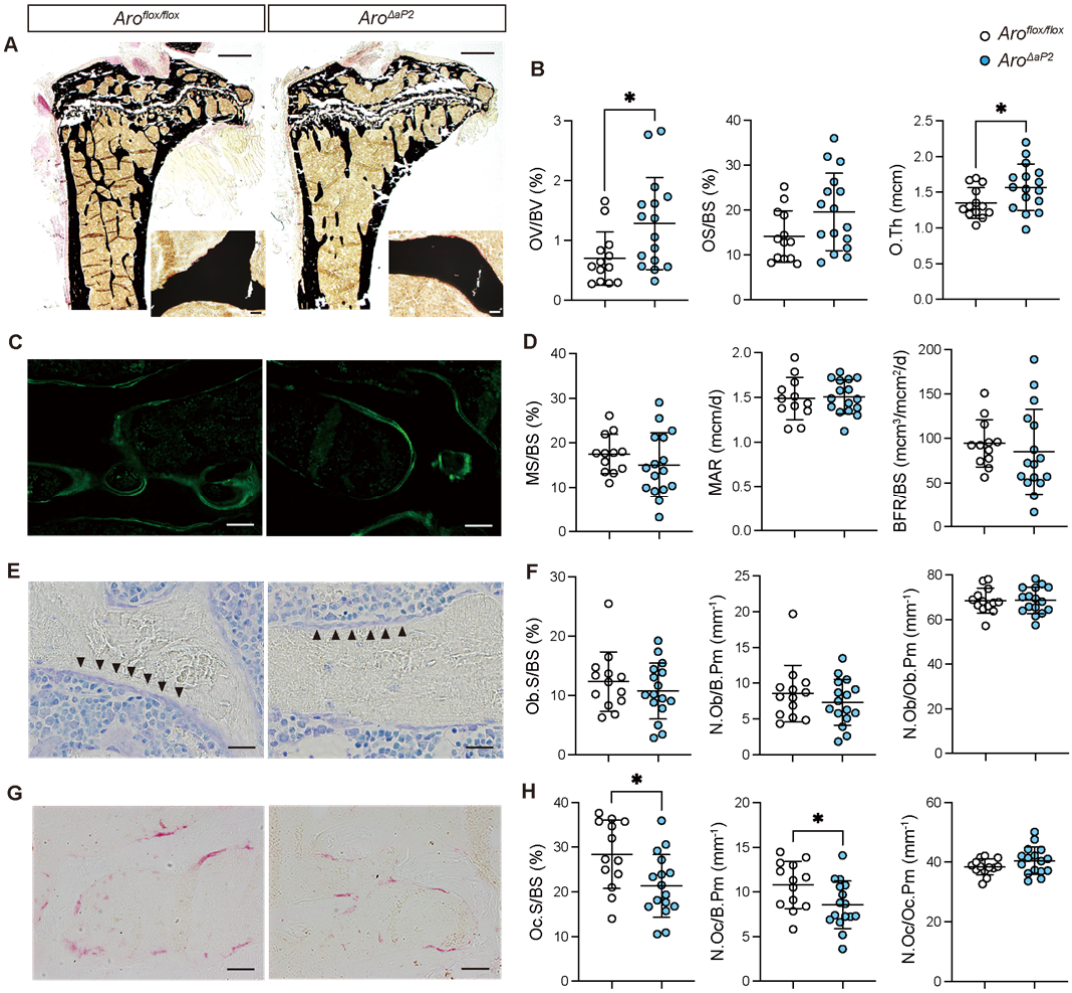

Figure 3. *Aro*$^{\Delta aP2}$ mice exhibited high osteoid volume and low osteoclast number. (A) Representative image of Von Kossa staining in the tibia. Scale bar of low magnification image indicates 500 μm. Scale bar of high magnification image indicates 20 μm. (B) Osteoid volume/bone volume (OV/BV), osteoid surface/bone surface (OS/BS), osteoid thickness (O.Th). (C) Representative image of calcein labeling in tibia. Scale bar indicates 100 μm. (D) Mineralizing surface (MS/BS), Mineral apposition rate (MAR), Bone formation rate (BFR/BS). (E) Representative image of Toluidine blue staining in tibia. Scale bar indicates 50 μm. (F) Osteoblast surface (Ob.S/BS), osteoblast number/bone perimeter (N.Ob/B.Pm), osteoblast number/osteoblast perimeter

745 (N.Ob/Ob.Pm). (G) Representative image of TRAP staining in tibia. Scale bar indicate
746 50 μm. (H) Osteoclast surface/bone surface (Oc.S/BS), osteoclast number/bone
747 perimeter (N.Oc/B.Pm), osteoclast number/osteoclast perimeter (N.Oc/Oc.Pm). Data are
748 presented as means ± SD. *, $p < 0.05$
749

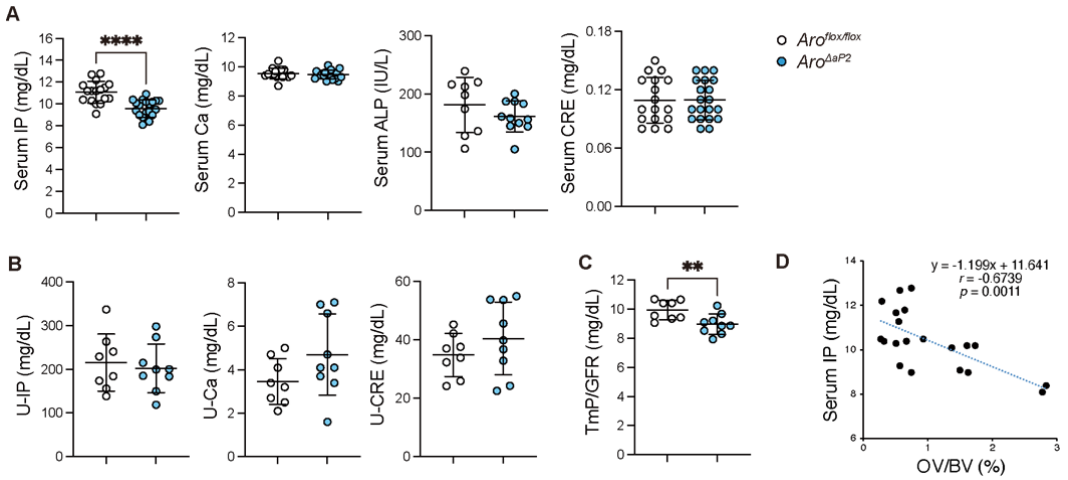

Figure 4. *Aro*$^{\Delta aP2}$ mice exhibited low serum phosphate and decreased urinary phosphate reabsorption. (A) Serum IP, Ca, ALP and CRE. (B) Urine IP, Ca, and CRE. (C) Tmp/GFR calculated by serum and urine parameters. (D) Correlation between serum IP and OV/BV. Data are presented as means ± SD. **, $p < 0.01$; ****, $p < 0.0001$.

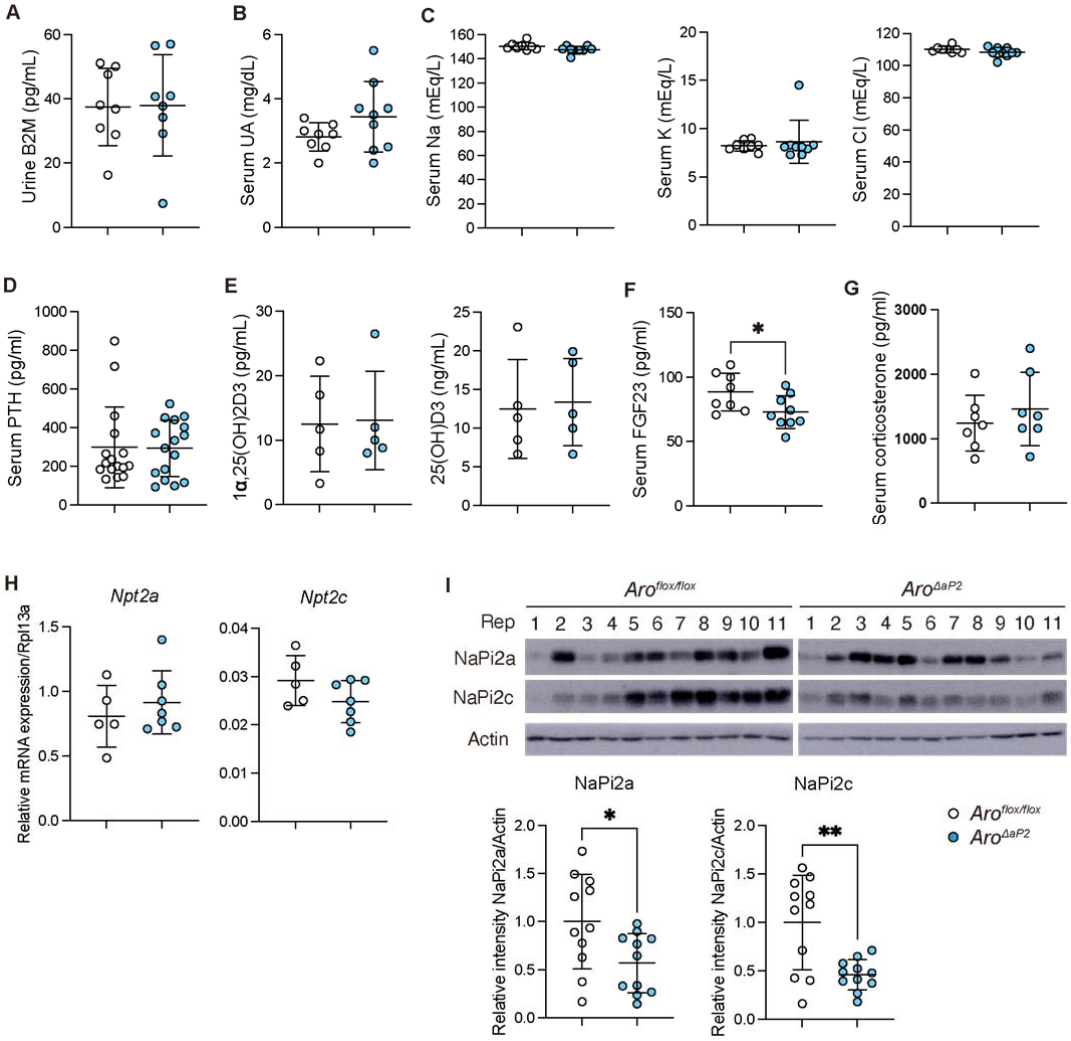

Figure 5. *Aro$^{\Delta aP2}$* mice exhibited low NaPi2a and NaPi2c protein levels in the kidney. (A) Urine B2M and (B) Serum UA as indicators for renal tubular damage. (C) Serum Na, K, and Cl as indicators for Fanconi syndrome. (D) Serum PTH, (E) 1α,25$(OH)_2D_3$, 25$(OH)D_3$, (F) FGF23, and (G) corticosterone as a phosphate metabolism regulating hormone. (H) Gene expression of *Npt2a* and *Npt2c* in the kidney. (I) Protein expression of NaPi2a and NaPi2c in renal BBMVs. Data are presented as means ± SD. *, $p < 0.05$; **, $p < 0.01$.

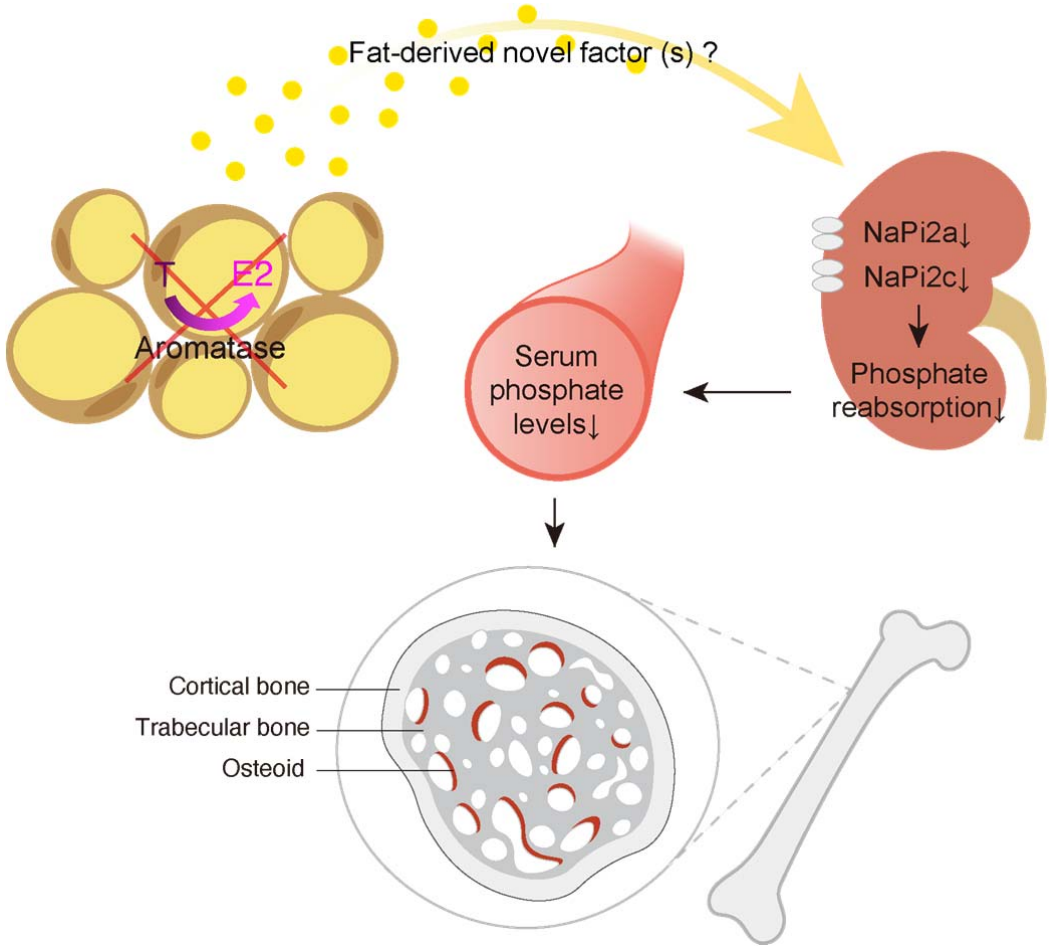

765

766 **Figure 6.** In *Aro*$^{\Delta aP2}$ mice, E2 biosynthesis by aromatase in adipose tissue was
767 suppressed, resulting in suppression of fat-derived novel factor (s) that regulates renal
768 NaPi2 protein levels, suppressing renal phosphate reabsorption and reducing serum
769 phosphate levels. As a result, *Aro*$^{\Delta aP2}$ mice exhibited an abnormal bone calcification
770 phenotype.

771